Active Targeting of Sorafenib: Preparation, Characterization, and In Vitro Testing of Drug-Loaded Magnetic Solid Lipid Nanoparticles

Agostina Grillone, Eugenio Redolfi Riva, Alessio Mondini, Claudia Forte, Lucia Calucci, Claudia Innocenti, Cesar de Julian Fernandez, Valentina Cappello, Mauro Gemmi, Stefania Moscato, Francesca Ronca, Rodolfo Sacco, Virgilio Mattoli, and Gianni Ciofani**

Sorafenib is an anticancer drug approved by the Food and Drug Administration for the treatment of hepatocellular and advanced renal carcinoma. The clinical application of sorafenib is promising, yet limited by its severe toxic side effects. The aim of this study is to develop sorafenib-loaded magnetic nanovectors able to enhance the drug delivery to the disease site with the help of a remote magnetic field, thus enabling cancer treatment while limiting negative effects on healthy tissues. Sorafenib and superparamagnetic iron oxide nanoparticles are encapsulated in solid lipid nanoparticles by a hot homogenization technique using cetyl palmitate as lipid matrix. The obtained nanoparticles (Sor-Mag-SLNs) have a sorafenib loading efficiency of about 90% and are found to be very stable in an aqueous environment. Plain Mag-SLNs exhibit good cytocompatibility, whereas an antiproliferative effect against tumor cells (human hepatocarcinoma HepG2) is observed for drug-loaded Sor-Mag-SLNs. The obtained results show that it is possible to prepare stable Sor-Mag-SLNs able to inhibit cancer cell proliferation through the sorafenib cytotoxic action, and to enhance/localize this effect in a desired area thanks to a magnetically driven accumulation of the drug. Moreover, the relaxivity properties observed in water suspensions hold promise for Sor-Mag-SLN tracking through clinical magnetic resonance imaging.

1. Introduction

Hepatocellular carcinoma (HCC) is the most common type of primary liver cancer, and it represents the third leading cause of cancer-related death worldwide.[1] The highest incidence rates are found in China (55% of the world total), Japan, Southeast Asia, and sub-Saharan Africa.[2] The risk factors increasing the incidence of HCC are hepatitis B and hepatitis C virus infections, alfa-toxin exposure, alcoholic cirrhosis, and cigarette smoking,[3,4] and the therapeutic strategy may change on the basis of the liver conditions and of the tumor stadiation.[5,6] Curative treatments, such as surgical resection, liver transplantation, and local ablation, can improve the survival of HCC patients at an early stage diagnosis; on the contrary, no effective treatments are available for patients with advanced HCC.

As HCC is highly resistant to chemotherapy, target therapies have been

A. Grillone, E. Redolfi Riva, Dr. A. Mondini, Dr. V. Mattoli, Dr. G. Ciofani
Istituto Italiano di Tecnologia
Center for Micro-BioRobotics @SSSA
Viale Rinaldo Piaggio 34, 56025 Pontedera, Pisa, Italy
E-mail: agostina.grillone@iit.it; gianni.ciofani@iit.it

A. Grillone, E. Redolfi Riva
Scuola Superiore Sant'Anna
The BioRobotics Institute
Viale Rinaldo Piaggio 34, 56025 Pontedera, Pisa, Italy

Dr. C. Forte, Dr. L. Calucci
Istituto di Chimica dei Composti OrganoMetallici
Consiglio Nazionale delle Ricerche – CNR
Via Giuseppe Moruzzi 1, 56124 Pisa, Italy

Dr. C. Innocenti
INSTM and Department of Chemistry "Ugo Shiff"
University of Florence
Via della Lastruccia 3–13, 50019 Sesto Fiorentino, Firenze, Italy

Dr. C. de Julian Fernandez
Istituto dei Materiali per l'Elettronica e il Magnetismo
Consiglio Nazionale delle Ricerche – CNR
Parco Area delle Scienze 37/A, 43124 Parma, Italy

Dr. V. Cappello, Dr. M. Gemmi
Istituto Italiano di Tecnologia
Center for Nanotechnology Innovation @NEST
Piazza San Silvestro 12, 56127 Pisa, Italy

Dr. S. Moscato
Dipartimento di Medicina Clinica e Sperimentale
Università di Pisa
Via Savi 10, 56126 Pisa, Italy

Dr. F. Ronca
Università di Pisa
Dipartimento di Patologia Chirurgica
Medica, Molecolare e dell'Area Critica
Via Savi 10, 56126 Pisa, Italy

Dr. R. Sacco
Unità Operativa di Gastroenterologia e Malattie del Ricambio
Azienda Ospedaliera-Universitaria Pisana
Via Paradisa 2, 56124 Pisa, Italy

DOI: 10.1002/adhm.201500235

evaluated as first-line treatment or combinational therapies.[7,8] Interesting perspectives seem to come from sorafenib (Bayer's proprietary compound BAY 43–9006), the first clinically approved drug for HCC and for advanced renal cell carcinoma (RCC).[9] Indeed, in vivo and in vitro studies have demonstrated that sorafenib is able to block the tumor growth by inhibiting important components of signaling pathways involved in the proliferation and in the angiogenesis of the tumor.[10] Sorafenib is a small molecule able to block cell surface tyrosine kinase receptors (e.g., vascular endothelial growth factor receptors VEGFR-2 and VEGRF-3, and platelet-derived growth factor receptor-β PDGFR-β, c-kit, and Flt-31) and, down-stream, intracellular serine/threonine kinases (e.g., Raf-1, wild-type B-Raf, and mutant B-Raf), the action of which, when not precisely regulated, may induce oncogenesis.[11] Although sorafenib is the only systemic therapy capable of increasing the overall patient survival, as well as of delaying the progression of the pathology in patients with advanced HCC, its severe side effects (as hand-foot skin reaction, decreased heart blood flow, heart attack, perforation of the bowel, change in thyroid hormone levels, loss of appetite, tiredness, diarrhea, rash, etc.) may eventually require the interruption of the treatment. Furthermore, the poor solubility of sorafenib in aqueous environments strongly limits its application for local treatment.[9]

All the mentioned drawbacks of sorafenib may be overcome by the use of nanovectors capable of selectively targeting and delivering the drug into the target tissue, for example, by exploiting magnetic transport granted by loading with superparamagnetic nanoparticles.[12] The aim of the proposed study is the development of a drug-loaded magnetic nanovector able to efficiently and selectively deliver sorafenib to the tumor site with the help of an external magnetic field. This system, targeting the drug to a specific area, would concentrate it in the intended site, thus increasing its efficacy and avoiding the administration to healthy tissues, with the consequence of reducing the aforementioned dangerous side effects.

The class of nanovectors used in this study is represented by solid lipid nanoparticles (SLNs), a drug delivery system composed of a solid lipid matrix stabilized by a surfactant in aqueous solution.[13] Thanks to the solid lipid matrix, SLNs present several benefits with respect to other types of carriers. In fact, they ensure a controlled release of the drug, protect the drug from degradation and metabolic inactivation, show a high drug loading efficiency, and finally are non-toxic at both cellular and systemic level. The lipid used in this study is cetyl palmitate, an ester manufactured from raw materials exploited in several cosmetic formulations.[14] The drug magnetic targeting is ensured by the presence of superparamagnetic iron oxide nanoparticles (SPIONs) within the lipid matrix, which render the SLNs magnetically responsive.[15–17] Moreover, based on the contrast properties shown by SPIONs,[18–21] our SLNs could be noninvasively tracked by means of magnetic resonance imaging (MRI) scanners.

Sorafenib and SPIONs were encapsulated in cetyl palmitate SLNs by a hot homogenization technique, and the obtained nanovectors (Sor-Mag-SLNs) were thoroughly characterized by determining size distribution, zeta potential, morphology, drug and SPION loading efficiency, and magnetic properties. Drug targeting and biological effects were tested in vitro on the human hepatocellular carcinoma cell line HepG2, taking advantage of a home-made dynamic culturing system. Moreover, longitudinal and transverse water proton relaxivities of aqueous suspensions of Sor-Mag-SLNs were investigated at two magnetic fields in order to preliminarily assess the potential negative contrast properties of the proposed nanovectors, in view of their possible application as theranostic nanoplatforms.

2. Results

2.1. Sorafenib-Loaded Magnetic Solid Lipid Nanoparticles

Sorafenib-loaded magnetic solid lipid nanoparticles (Sor-Mag-SLNs), prepared by a hot homogenization technique using cetyl palmitate as lipid matrix, as depicted in the schema of **Figure 1**, presented an average diameter of 248 ± 113 nm (dynamic light scattering measurement, DLS) and a *Z*-potential value of –23.0 ± 5.3 mV. These data indicate a good colloidal stability of the nanoparticles in aqueous environment, which prevents aggregation during all the experiments. Moreover, a satisfactory polydispersity index was determined (0.2 ± 0.1), thus suggesting monodisperse nanoparticle size distribution.

Atomic force microscopy (AFM) scans confirm a regular spherical shape of Sor-Mag-SLNs, characterized by an average diameter of 420 ± 181 nm, calculated via software analysis (**Figure 2**a,b). This value is over-estimated with respect to DLS measurements, most probably because of the collapse and spreading of cetyl palmitate onto the substrate after water evaporation, as well as of the interaction of the cantilever with the nanoparticle edges. In the topographical scans of single nanoparticles it is possible to observe an irregularly shaped area at the center of the circular edge, better evidenced by the 3D rendering of the scan (Figure 2c), which is probably due to drug and magnetic nanoparticle entrapment inside the SLNs. Moreover, a displacement in the oscillation phase of the cantilever is evidenced in AFM tapping phase scans (see Figure S1, Supporting Information) when the tip interacts with the two aforementioned portions of the nanoparticles evidenced by topographical scans. These results collectively indicate that the nanoparticles are composed of materials characterized by different mechanical properties, thus suggesting the presence of SPIONs inside the lipid core.

The presence of magnetic nanoparticles, characterized by different electron density and encapsulated in the lipid matrix, is in fact confirmed by transmission electron microscopy (TEM) images (Figure 2d,e), where it is clearly possible to discern both internalized SPIONs (Figure 2d) and SPIONs on the SLN surface (Figure 2e).

The loading of SPIONs on SLNs was investigated by thermogravimetric analysis (TGA) and elemental analysis performed by inductively coupled plasma-mass spectrometry (ICP-MS). From the comparison of the thermal degradation behaviors under air flow (see Figure S2, Supporting Information) a SPION loading of about 3 wt% could be estimated. In agreement, elemental analysis gave an iron content of 1.4 wt%.

Concerning magnetic properties, Sor-Mag-SLNs present a superparamagnetic behavior at room temperature, as the coercive field of about 200 Oe at 5 K becomes negligible at 300 K.

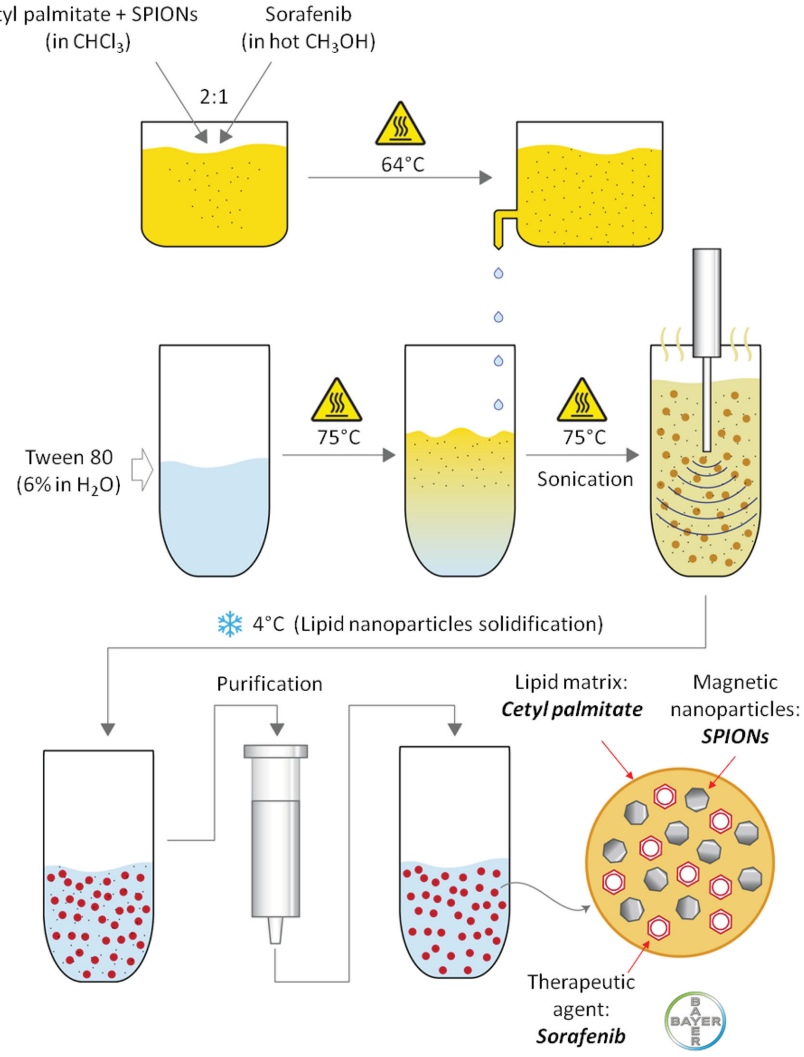

Figure 1. Schematization of the procedure followed for the preparation of sorafenib-loaded magnetic solid lipid nanoparticles (Sor-Mag-SLNs).

This observation was confirmed by the zero field cool (ZFC)/field cool (FC) curve at 25 Oe, as the blocking temperature is around 190 K (**Figure 3**a). The lower blocking temperature of Sor-Mag-SLNs with respect to SPIONs and the broadening of the ZFC curve are hints of less inter-domains interactions because of the presence of the lipid matrix.

The hysteresis curves of the two materials are similar (Figure 3b), thus indicating analogous magnetic properties. Sor-Mag-SLNs present a higher coercive field, again because of the encapsulation of SPIONs inside the lipid matrix. The magnetic saturation value of Sor-Mag-SLNs is about 1.95 emu g^{-1} at 300 K (60 emu g^{-1} for SPIONs), while 2.3 emu g^{-1} at 5 K (70 emu g^{-1} for SPIONs). Considering that the magnetic moment *per* particle should not be different between SPIONs and Sor-Mag-SLNs, we can conclude that the percentage in mass of iron oxide nanoparticles in the solid lipid particles is about 3%, in agreement with thermogravimetric and elemental analyses. On the other hand, the magnetization of the Sor-Mag-SLNs is almost saturated with a low magnetic field, i.e., 1000 Oe. This assures the easy manipulation of the magnetic nanovectors by an external magnetic field.

Quantitative information on longitudinal (r_1) and transverse (r_2) relaxivities of Sor-Mag-SLNs at 0.47 and 7.05 T at 37 °C was acquired from measurements of water proton T_1 and T_2 relaxation times on aqueous suspensions at different concentrations. In all cases, a linear dependence was found between relaxation rates ($R_1 = 1/T_1$ and $R_2 = 1/T_2$) and nanoparticle concentration. The relaxivity values, determined by fitting these data and considering the Fe concentration in Sor-Mag-SLNs determined by elemental analysis, and their ratio (r_2/r_1) are reported in **Table 1** together with relaxivities of commercial contrast agents based on SPIONs. These results indicate that Sor-Mag-SLNs have good negative contrast properties at the investigated fields, in particular showing r_2 (38 ± 2 s^{-1} m M^{-1} at 7.05 T, 215 ± 5 s^{-1} m M^{-1} at 0.47 T) and r_2/r_1 (633 at 7.05 T, 77 at 0.47 T) values much higher than commercial agents at magnetic fields of clinical interest.[22–26]

Successful sorafenib loading inside magnetic SLNs was assessed by UV–vis quantification of the drug, the estimated loading efficiency being about 90%, corresponding to a sorafenib concentration of 6.35×10^{-6} M in 200 µg mL^{-1} samples of Sor-Mag-SLNs. Interestingly, drug release investigations performed at different pH values (3, 7, and 10) revealed no significant, extremely slow, release of sorafenib (less than 5% after 10 d, Figure S3, Supporting Information). These data suggest as biological effects, described in Sections 2.2. and 2.3., are ascribable to the degradation of cetyl palmitate by intracellular enzymes upon cellular internalization, and consequent release of the active drug from the dissolving lipid matrix.

2.2. In Vitro Cytotoxicity Study

Antitumor activity of Mag-SLNs and Sor-Mag-SLNs was investigated against HepG2 cells with the WST-1 viability assay and compared to that of the free-administered drug. As shown in **Figure 4**, Mag-SLNs did not significantly inhibit cell viability after both 24 h (Figure 4a) and 72 h (Figure 4b) of incubation (at all the investigated concentrations $p > 0.05$ with respect to the controls). On the other hand, Sor-Mag-SLNs showed a moderate cytotoxic effect after 24 h of incubation. In fact, for Sor-Mag-SLNs concentrations of 50, 100, and 200 µg mL^{-1}, corresponding to 1.60×10^{-6}, 3.19×10^{-6}, and 6.35×10^{-6} M of sorafenib, a viability reduction of about 15% was observed, which, however, is not statistically significant (Figure 4a). A strong dose-dependent antiproliferative effect was instead

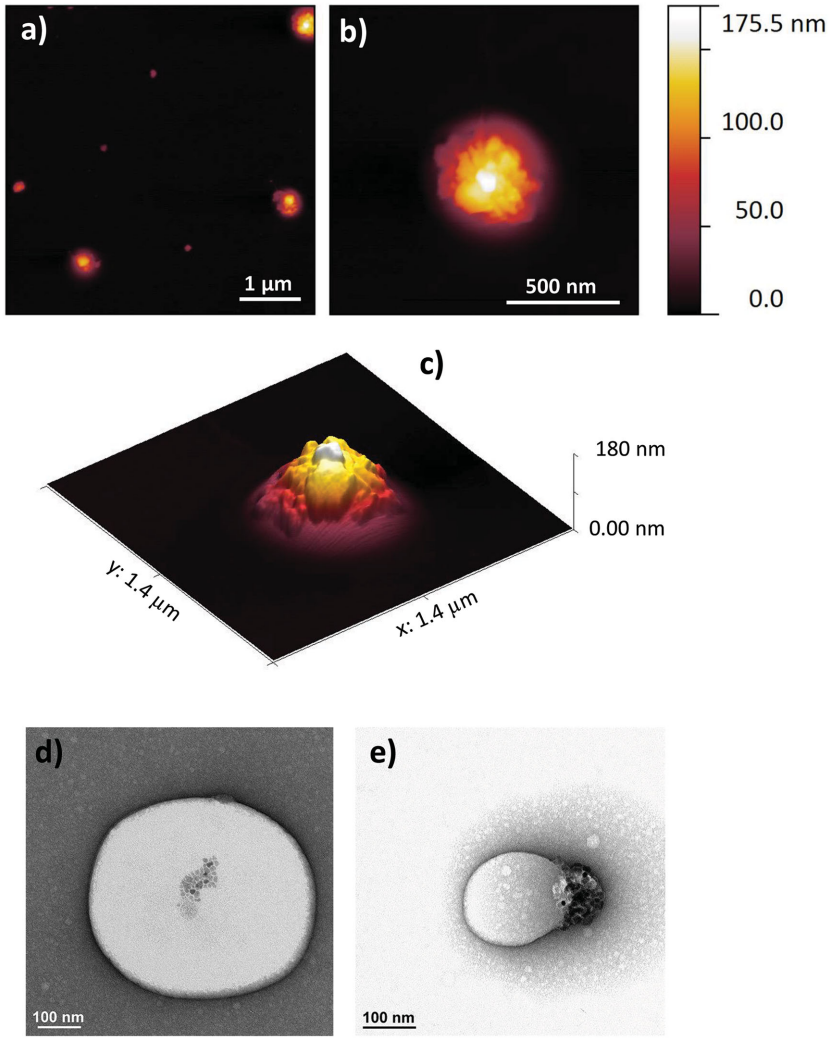

Figure 2. AFM and TEM imaging of Sor-Mag-SLNs. AFM topographical scans at a) low and b) high magnification of nanoparticles deposited onto a silicon substrate; c) 3D rendering of an AFM scan; d,e) TEM images of nanoparticles.

observed after 72 h of incubation (Figure 4b): at all the tested concentrations we have a significant reduction of viability ($p < 0.05$), that reaches about 40% of the control for the 200 µg mL^{-1} Sor-Mag-SLN concentration (6.35×10^{-6} M of sorafenib).

The free drug confirmed its antitumor action both at 24 h (for concentrations of 1.60, 3.19, and 6.35×10^{-6} M, $p < 0.05$) and at 72 h (for concentrations of 3.19 and 6.35×10^{-6} M, $p < 0.05$).

Overall, these results indicate good cytocompatibility of the plain Mag-SLNs; conversely, drug-loaded Sor-Mag-SLNs show an antiproliferative effect against tumor cells similar to that induced by free sorafenib, thus demonstrating their ability to deliver active drug into the cells.

These quantitative results were confirmed by the Live/Dead viability/cytotoxicity assay (see Figure S4, Supporting Information). Also in this case, the cytocompatibility of Mag-SLNs was optimal at the tested concentration (200 µg mL^{-1}). No evidence of cell membrane damage was observed after the treatment, demonstrating the high viability of cells after 72 h of incubation with the plain nanoparticles, in line with non-treated control cultures. On the contrary, Sor-Mag-SLNs exercised a significant cytotoxic effect at the same concentration (200 µg mL^{-1}, corresponding to 6.35×10^{-6} M of drug), as demonstrated by the great amount of red-stained cells observed at the end of the 72 h treatment. Once again, similar results were achieved with the same concentration of free drug (6.35×10^{-6} M).

Finally, based on observations from the literature, that reported as treatment with sorafenib increases Erk1 and Erk2 phosphorylation,[27] we assessed phosphorylated Erk1/2 (pErk1/2) expression in HepG2 treated with sorafenib (6.35×10^{-6} M) or Sor-Mag-SLNs (200 µg mL^{-1}, corresponding to 6.35×10^{-6} M of drug). Coherently with those findings, **Figure 5** shows increased pErk1/2 expression in cells treated with sorafenib or Sor-Mag-SLNs, which is more evident at 72 h of incubation compared to the controls. In agreement with data on cell viability, we observed that the cytotoxic effect of sorafenib and Sor-Mag-SLNs correlates with an increase of pErk1/2 in HepG2 cells rather than with an inhibition as reported in other studies: further investigations will be thus needed to verify whether the activation of the MAP kinase pathways is independent from the cytotoxic effect of sorafenib.[28]

Taken together, all these data demonstrate that Sor-Mag-SLNs represent an excellent vector for sorafenib delivery, thanks to the nanoparticle biocompatibility and the retention of the drug activity following encapsulation.

2.3. Cellular Uptake Studies and Magnetic Drug Targeting

Cellular internalization studies revealed strong uptake of Sor-Mag-SLNs by HepG2 cells; a 3D confocal rendering of a cell internalizing the nanoparticles is reported in the Supporting Information, as Video S1. Moreover, staining of lysosomes allowed a significant colocalization to be demonstrated, thus corroborating the hypothesis of drug release following the degradation of the lipid matrix in these digestive organelles. In **Figure 6**, Sor-Mag-SLNs are stained in red, Lysotracker probe is green-fluorescent, and overlapping is easily evidenced by the yellow signal arising from the merging of the two channels (Pearson's index $R = 0.67$).

Magnetic targeting experiments were performed in dynamic conditions thanks to the set-up depicted in **Figure 7**a, as widely described in the Experimental Section. Results show an enhanced Sor-Mag-SLNs uptake by cells cultured in correspondence of the region of the microfluidic channel where the external permanent magnet was placed (Figure 7b). Conversely,

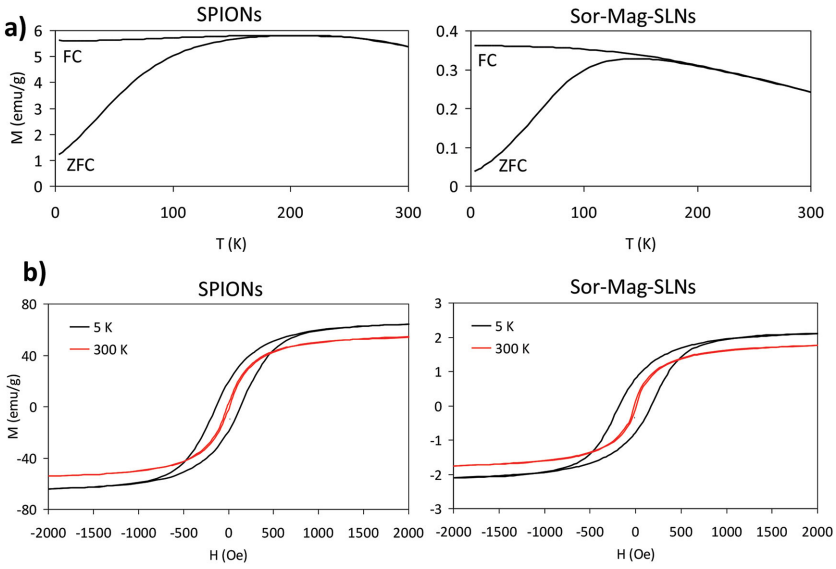

Figure 3. Magnetic characterization. a) Temperature dependence of the ZFC and FC magnetizations measured with a magnetic field of 25 Oe and b) hysteresis curves acquired at 5 and 300 K.

no significant nanoparticle internalization can be appreciated in cells cultured in the control channel (i.e., without the presence of the magnet), thus demonstrating the possibility of actively targeting the nanoparticle uptake and, consequently, of selectively localizing the effect of the drug.

The possibility of magnetically targeting the drug effects was in fact demonstrated by testing the Sor-Mag-SLNs efficiency in dynamic conditions through the Live/Dead viability/cytotoxicity assay performed 72 h after the targeting experiment. **Figure 8**a in fact shows a substantial increase of dead red-stained cells in correspondence of the channel where the magnetic accumulation of Sor-Mag-SLNs occurred; conversely, cells cultured in the control channel showed optimal viability, with no sign of toxicity induced by the drug. This qualitative evidence was confirmed by the quantitative determination of cell mortality, evaluated as percentage of cells positive for EthD-1, which resulted to be about 95% in the channel close to the magnet, and 5% in the control compartment (Figure 8b).

Table 1. Longitudinal and transverse relaxivity values of Sor-Mag-SLNs and some commercial SPION-based contrast agents.

Sample	Field [T]	T [°C]	r_1 [s^{-1} mM^{-1}]	r_2 [s^{-1} mM^{-1}]	r_2/r_1
Sor-Mag-SLNs	7.05	37	0.06 ± 0.02	38 ± 2	633
Feridex[22]	7	–	–	166.71	–
Molday ION[23]	7	–	–	106 ± 4	–
Feratrack[22]	7	–	–	247 ± 14	–
Sor-Mag-SLNs	0.47	37	2.80 ± 0.05	215 ± 5	77
Endorem (AMI-25)[24]	0.47	37	27 ± 1	152 ± 8	5.6
Endorem (AMI-25)[24]	0.47	39	23.7 ± 1.2	107 ± 11	4.5
Ferumoxsil[25]	0.47	39	3.2 ± 0.9	72 ± 12	22.5
Resovist (SHU-555A)[24]	0.47	37	20.6 ± 1.0	86 ± 4	4.2
Resovist (SHU-555A)[26]	0.47	37	24.9	177	7.1
Sinerem (AMI 227)[25]	0.47	39	22.7 ± 0.2	53.1 ± 3.3	2.34

3. Discussion

Magnetic nanovectors for drug delivery/targeting have been proposed for a wide range of applications in the literature, but indeed only a few studies of nanotheranostics have been successfully carried out in preclinical models.[29] The needing of improved formulations, strategies, and personalized approaches is still pressing and challenging. Despite some encouraging results,[30,31] we are still far to find an ideal vector, and often combined strategies and solutions dedicated to the specific considered application are needed to be elaborated. In the design of a new magnetic nanovector, envisaged for both therapeutic and diagnostic purposes, optimizations and compromises among several features should be achieved, in particular in terms of stability, drug loading efficiency, imaging contrast efficiency, drivability, and targeting abilities, always taking into account the necessity of translate obtained results into a clinical scenario.

In this work, a novel approach to actively target sorafenib by encapsulation in magnetic solid lipidic nanoparticles, prepared through a hot oil-in-water homogenization process, was exploited. In particular, we focused on the problems encountered in the clinical use of sorafenib, consisting into the difficulty of localizing its effect, into its poor solubility in aqueous environment, and into its high toxicity for healthy tissues and organs. In this scenario, encapsulation of the drug in nanocarriers certainly represents an advantageous approach to reduce undesired side-effects, and to improve drug pharmacokinetics.[32–34]

A limited number of examples of sorafenib-loaded nanovectors can be found in the literature, including dextran/poly(*dl*-lactide-*co*-glycolide) block copolymer nanoparticles,[35] porous silicon nanoparticles,[36] lipid nanoparticles,[37] lipid-coated nanodiamonds,[38] dual polymeric-lipid nanoparticles,[39] PLGA microspheres,[40] and liposomes.[41] Worth to be mentioned is the work of Zhang et al.,[42] where sorafenib was loaded into magnetic folate-functionalized polymeric micelles, and the targeting ability of the proposed nanovectors, due to the presence of folate molecules, was demonstrated, but active magnetically-driven guidance was not investigated. On the other hand, SPION coencapsulation into the micelles allowed the nanoparticles to be localized by MRI.

In our study, we have chosen solid lipid nanoparticles for sorafenib encapsulation and selective delivery because of a series of advantages they offer with respect to other types of nanocarriers. These include the absence of undesired acid degradation products,[43] the higher drug loading capability (we achieved a 90% of drug encapsulation), the stronger drug/matrix interaction,[44,45] and the possibility of an easy scale-up

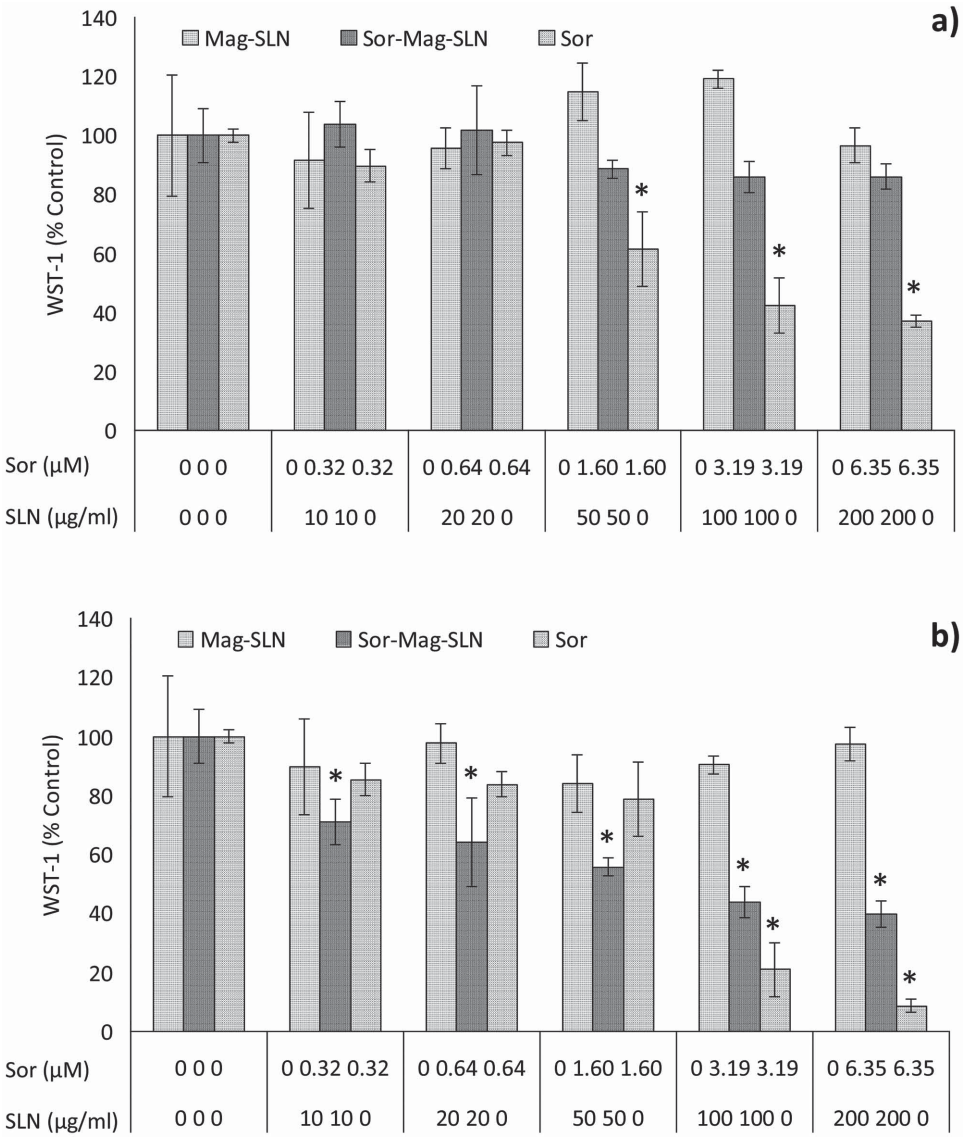

Figure 4. Metabolic WST-1 assay on HepG2 cells after a) 24 h and b) 72 h of incubation with increasing concentrations of Mag-SLNs, Sor-Mag-SLNs, and free sorafenib. * $p < 0.05$.

of the SLN production.[46] Furthermore, exploiting the simultaneous encapsulation of SPIONs in the SLNs, we addressed another main problem of sorafenib and, more generally, of traditional chemotherapy, i.e., the difficulty to restrict the drug cytotoxic effect to a desired target area. Indeed, SPIONs confer a magnetic moment to our nanovectors, and thus enable their movement/targeting in the presence of a remote static magnetic field. Moreover, thanks to the magnetic SLN relaxivity properties, also arising from the encapsulation of SPIONs, our nanoparticles can be also envisaged as negative contrast agents to be tracked through MRI, with features superior to those of other commercially available systems (Table 1). In this view, the developed system holds promise as an actual theranostic platform, able to provide both therapy and imaging in a single device.[47–50]

Of course, the potential application of Sor-Mag-SLNs in theranostics requires the assessment of targeted therapy and tracking under MRI in vivo, and future investigations are planned to address these issues.

4. Conclusion

In this study, we demonstrated the possibility to successfully encapsulate sorafenib in magnetic solid lipid nanoparticles by an oil-in-water homogenization process at high temperature, using cetyl palmitate as lipid matrix. Sorafenib-loaded magnetic SLNs show optimal morphological stability with a regular spherical shape and an average diameter of less than 300 nm. The prepared nanovectors are able to inhibit HepG2 cancer cell proliferation through the sorafenib cytotoxic effect, and to focus this effect on a desired area thanks to their magnetically driven accumulation. Moreover, modification of the SLN surface, through the grafting of ligands recognizing specific cancer cell

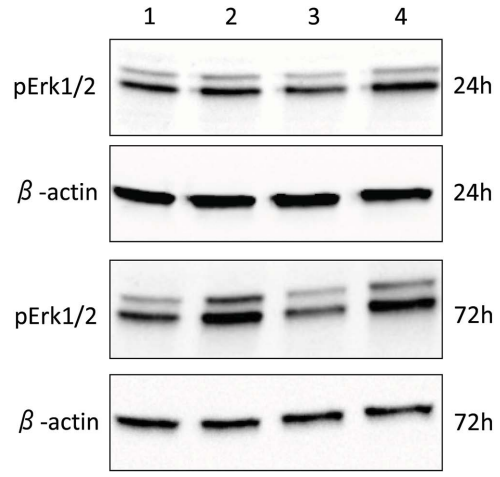

Figure 5. Western blotting analysis for pErk1/2 (and β-actin as control) expression on HepG2 cellular lysates after 24 and 72 h of incubation in control cultures (lane 1) and in cultures treated with free sorafenib 6.35×10^{-6} M (lane 2), Mag-SLNs 200 μg mL^{-1} (lane 3), or Sor-Mag-SLNs 200 μg mL^{-1} (lane 4).

receptors, could be envisaged in order to make these nanovectors even more specific toward the desired target.

Sorafenib-loaded magnetic solid lipid nanoparticles represent a good example of nanodevice in the field of oncology. Their potential dual function, as both negative contrast agent and therapeutic agent, make them a promising theranostic tool for the treatment of cancer, and future experiments will be performed to study the performance of the proposed nanoplatform in vivo.

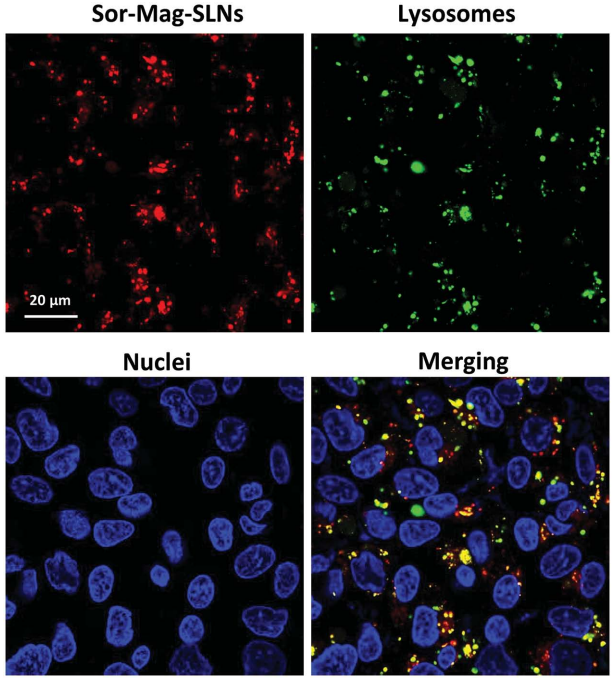

Figure 6. Investigation of cellular uptake. Confocal fluorescence images of HepG2 cells showing Sor-Mag-SLN uptake (in red) and colocalization with lysosomes (in green) after LysoTracker assay; nuclei counterstained in blue.

5. Experimental Section

Solid Lipid Nanoparticle Preparation and Characterization: Solid lipid nanoparticles loaded with sorafenib and SPIONs (Sor-Mag-SLNs) were prepared by using an oil-in-water homogenization process at high temperature. In detail, 5 mg of sorafenib tosylate (kindly provided by Bayer International) were dissolved in 500 μL of hot methanol (65 °C). Meanwhile, 210 mg of cetyl palmitate (kindly provided by Gattefossé) and 15 mg of SPIONs (average diameter of 10 nm, EMG1300 from Ferrotec) were dissolved in 1 mL of chloroform. The methanol and chloroform solutions were added and gently stirred. The obtained mixture was then transferred into a vial containing 3 mL of a Tween 80 (Sigma-Aldrich) water solution (6%), and sonicated for 5 min with a probe-tip ultrasonicator (SONOPLUS mini20, Bandelin). To allow organic solvents evaporation, the temperature of the emulsion was kept constant at 75 °C using a home-made heating system with a negative feedback control. Briefly, two thermoelectric coolers were assembled onto a precut metallic tube holder and connected to a software programmable feedback system, which ensures accurate temperature control (see Figure S5, Supporting Information, for details). At the end of the procedure, the obtained dispersion was maintained at 4 °C for 15 min to allow the formation of the SLNs. In order to remove the surfactant, solvent residuals, and non-encapsulated drug and SPIONs, the final product was purified by gel chromatography, using Sephadex G-25 prepacked columns (GE Healthcare Life Sciences) with deionized water as eluent. Plain magnetic SLNs (Mag-SLNs), i.e., not loaded with sorafenib, were prepared following the same procedure, but omitting the drug, and were used as controls in biological experiments. A scheme of the above described procedures is provided in Figure 1. Sor-Mag-SLN characterization in terms of size and *Z*-potential was performed through dynamic light scattering with a Malvern Zetasizer Nano S90. The morphology of Sor-Mag-SLNs was investigated by AFM with an Innova SPM (Bruker), after drying a drop of appropriately diluted nanoparticle dispersion onto a silicon wafer. AFM scans were performed in tapping mode, by using NT-MDT NSG01 antimony-doped *n*-type silicon probes with a resonance frequency of 87–230 kHz and a force constant of 1.45–15.1 N m^{-1}. All data scans were elaborated and analyzed with the Gwyddion SPM analysis tool (http://gwyddion.net). TEM was moreover performed. Samples underwent negative staining, the simplest and fastest method for the surface characterization of particulate samples. We used a two-step protocol for the specimens preparation, which consists in a 30 s adsorption of a properly diluted Sor-Mag-SLN suspension over carbon-coated 300 mesh grids (EMS) followed by MilliQ water washing (three times), and by a 30 s staining with 3% uranyl acetate solution in ethanol. Grids were dried before observation, carried out with a Zeiss Libra 120 Plus transmission electron microscope operating at 120 kV, equipped with an in-column omega filter, and mounted with a 16-bit 2k × 2k CCD camera. For drug loading determination, freeze-dried Sor-Mag-SLNs were dissolved in hexane, in order to solubilize the lipid matrix, and sorafenib was extracted with DMSO. The sorafenib concentration was then estimated by UV–vis spectroscopy (NanoDrop, Thermo Scientific) exploiting the absorbance peak at 254 nm.[51] Drug release investigation was performed placing a Sor-Mag-SLN suspension (600 μL, concentration 10 mg mL^{-1}, corresponding to 320×10^{-6} M of drug) into dialysis bags (molecular weight cut-off 3.5 kDa, Sigma), immersed in a release bulk constituted by 3 mL of PBS at different pH conditions (3, 7, 10). The drug release study was carried out at 37 °C in a thermostatic shaker at a rate of 150 rpm. At predetermined time points, release bulk was replaced with fresh buffer solution, and aliquots freeze-dried; sorafenib was thereafter extracted in DMSO and its concentration assessed as previously described. TGAs were performed under air at a heating rate of 10 °C min^{-1} from 30 to 900 °C, by using a TG/DTA 7200 Extar instrument (SII Nanotechnology Inc). The iron content was measured by elemental analysis performed through ICP-MS using a Perkin Elmer NexION 300 spectrometer. Sample digestion was performed with 65% HNO_3 and 30% H_2O_2 in a Milestone Start D microwave apparatus.

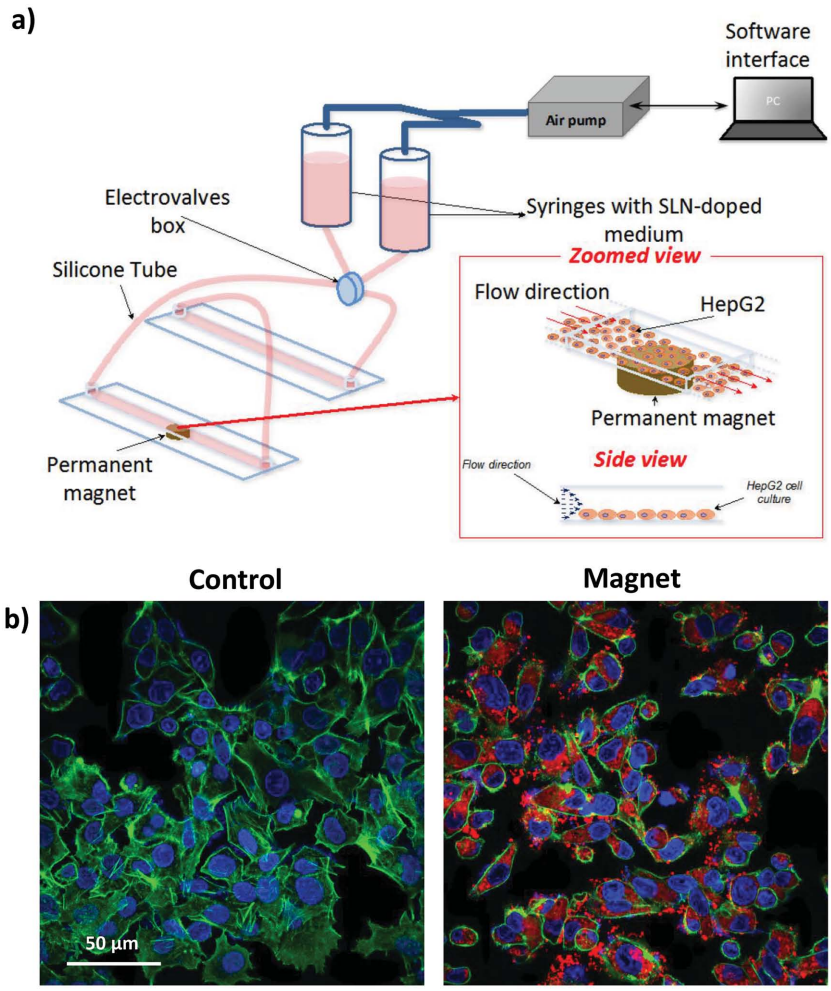

Figure 7. a) Schematization of the set-up exploited for dynamic magnetic targeting experiments. b) Results show enhanced Sor-Mag-SLN internalization in correspondence of the region of the microfluidic channel where the external magnet was placed with respect to the control channel; Sor-Mag-SLNs in red; f-actin in green; nuclei in blue.

Magnetic and Relaxometric Characterizations: Magnetic characterization was carried out using a superconducting quantum interference device (SQUID) from Quantum Design. Magnetization curves were measured from −50 to 50 kOe at 5 K and 300 K upon zero field cooling. The temperature dependence of the ZFC and FC magnetizations were recorded applying a probe field of 25 Oe to measure the thermal dependence of the magnetization and evaluate the superparamagnetic behavior of the nanoparticles. Measurements of water proton relaxation times (T_1 and T_2) were carried out at 37 °C on Sor-Mag-SLNs aqueous suspensions at different concentrations obtained by dilution of a 30 mg mL^{-1} mother suspension with ultrapure water. Measurements at 20 MHz (0.47 T) were performed with a Spinmaster FFC-2000 Fast Field-Cycling NMR relaxometer (Stelar). The temperature of the samples was controlled within ±0.2 °C with a Stelar VTC90 variable temperature controller. In particular, T_1 measurements were performed using the nonpolarized (NP) pulse sequence, while T_2 measurements were performed using the nonpolarized Carr–Purcell–Meiboom–Gill (NPCPMG) pulse sequence with a τ delay of 30 µs.[52] The 90° pulse duration was 9.7 µs. All the ^{1}H magnetization curves versus time were monoexponential within experimental error and the errors in fitting T_1 and T_2 were always less than 1%. Measurements of water proton T_1 and T_2 at 300.13 MHz (7.05 T) were performed with a Bruker AMX300 spectrometer using the Inversion Recovery pulse sequence and the CPMG pulse sequence[53,54] (τ = 100 µs) for T_1 and T_2 measurements, respectively. The 90° pulse duration was 6.7 µs. Relaxation rates (R_1 and R_2) were calculated as the inverse of the relaxation times ($R_1 = 1/T_1$ and $R_2 = 1/T_2$) and relaxivity values (r_1 and r_2) were determined on the basis of the iron concentration [Fe] of the samples, by fitting data acquired on Sor-Mag-SLN aqueous suspensions at different concentrations to the equation

$$R_i = R_{i0} + r_i \cdot [\mathrm{Fe}] \quad (1)$$

where i = 1,2 and R_{i0} is the R_i value of water alone.

Cell Cultures and In Vitro Cytotoxicity Study: Human hepatocellular carcinoma cell line (HepG2) was purchased by Sigma-Aldrich (85011430). HepG2 cells were cultured in low glucose Dulbecco's modified Eagle medium (DMEM) containing 10% of fetal bovine serum (FBS), 1% of non-essential amino acid solution (NEAAS), and 1% of penicillin-streptomycin, at 37 °C and in 5% CO_2 humidified atmosphere. In order to assess the biocompatibility of Mag-SLNs and the cytotoxic effects of free sorafenib and of Sor-Mag-SLNs against HepG2 cells, the WST-1 assay was performed (2-(4-iodophenyl)-3-(4-nitophenyl)-5-(2,4disulfophenyl)-2H-tetrazolium monosodium salt, provided in a pre-mix electrocoupling solution, BioVision). The cells were seeded at a density of 3 × 10^4 cells/well in 24-well plates and incubated for 48 h at 37 °C and 5% CO_2 in order to reach confluence. The medium was thereafter replaced with fresh medium containing increasing concentrations of Mag-SLNs (0, 10, 20, 50,100, and 200 µg mL^{-1}), Sor-Mag-SLNs (0, 10, 20, 50, 100, and 200 µg mL^{-1}), or sorafenib at concentrations equal to those present inside Sor-Mag-SLNs (0, 0.32, 0.64, 1.60, 3.15, 6.35 × 10^{-6} M). Cell viability was assessed after 24 and 72 h following the WST-1 protocol: culture medium was replaced with 300 µL of medium + 30 µL of the premix solution, and incubated for 1.5 h. Finally, the absorbance was read at 450 nm with a microplate reader (Victor3, Perkin Elmer). Cytotoxic effects of Sor-Mag-SLNs (200 µg mL^{-1}) were also qualitatively investigated at 72 h with the Live/Dead viability/cytotoxicity kit (Molecular Probes), that allows live cells (stained in green by calcein) to be discriminated from dead cells (stained in red by ethidium homodimer-1, EthD-1). The cells were rinsed with PBS, treated for 5 min at 37 °C with calcein AM, EthD-1, and Hoechst 33342 (H1399 Invitrogen, for nucleus counterstaining) in growth medium following manufacturer's instruction, and finally observed with an inverted fluorescence microscope (TE2000U, Nikon), equipped with a cooled CCD camera (DS-5MC USB2, Nikon) and with NIS Elements imaging software for image acquisition.

Western Blotting Analysis: In order to investigate the molecular mechanism of action of free sorafenib and Sor-Mag-SLNs, HepG2 whole cellular lysates were examined through Western blotting analysis for the detection of phosphorylated Erk1/2 (pErk1/2). Analysis were performed after 24 and 72 h of treatment using the concentration that showed the highest cytotoxic effect observed with the WST-1 test, i.e., 200 µg mL^{-1} of Sor-Mag-SLNs, corresponding to 6.35 × 10^{-6} M of drug. Mag-SLNs (200 µg mL^{-1}) were considered as well, as negative control. Briefly, HepG2 were cultured on Petri dishes at a density of 15 × 10^3 cells cm^{-2} for 24 h and then treated as described above. After 24 or 72 h treatment, cells were washed with D-PBS containing 1 × 10^{-3} M Na_3VO_4 and resuspended in a cell lysis ice-cold buffer (50 × 10^{-3} M Tris-HCl, 154 × 10^{-3} M NaCl, 20 × 10^{-3} M NaF, 1 × 10^{-3} M Na_3VO_4, 1 × 10^{-3} M EDTA, 1% NP40 and 1× of protease inhibitor cocktail, by

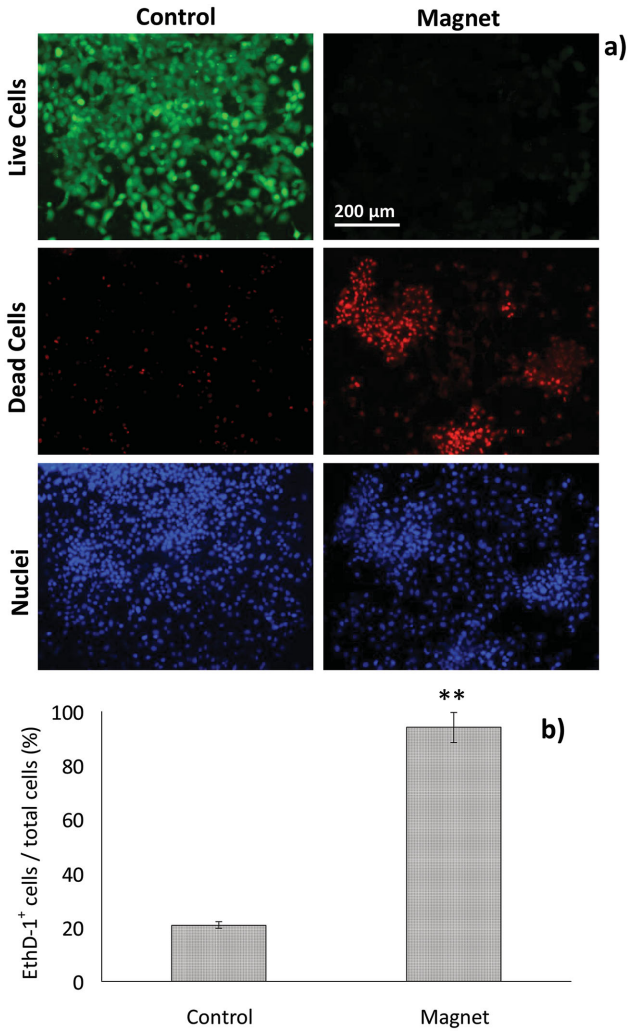

Figure 8. Selective drug action. a) Results of the Live/Dead viability/cytotoxicity assay following the magnetic targeting of Sor-Mag-SLNs; b) quantitative evaluation of cell mortality. ** $p < 0.001$.

Sigma-Aldrich). Samples were then disrupted using two 30 s pulses applied with the Micro-Ultrasonic Cell Disrupter (Vineland) set at 50% output in an ice bath. Sample lysates were centrifuged at 15 000 rpm for 20 min at 4 °C, and protein concentration in the supernatants was determined by the bicinchoninic acid microplate method, following manufacturer's instructions (Pierce). Proteins (20 µg lane^{-1}) were separated on a 10% polyacrylamide gel (Bio-Rad) under reducing conditions, and then transferred to a nitrocellulose membrane (Trans Turbo Blot system, Bio-Rad). The membrane was blocked with 3% bovine serum albumin in 0.1% Tween/Tris Buffer Saline (T-TBS) and incubated overnight at 4 °C with anti-pErk1/2 mouse monoclonal antibody (sc-7383, Santa Cruz) diluted 1:1000 in T-TBS. Anti β-actin mouse monoclonal antibody (A-5316, Sigma-Aldrich) was used as protein loading control. Anti-mouse Horse Radish Peroxidase (HRP)-conjugated antibodies (KPL), diluted 1:2000 in 4% dry nonfat milk in T-TBS for 1 h at room temperature, was used as secondary antibody, and the immunocomplexes were detected by chemiluminescence (ECL clarity, Bio-Rad) by using a Chemi-Doc XRS+ system (Bio-Rad). The data were analyzed by using Image Lab software (Bio-Rad).

Cellular Uptake Investigation: Internalization of SLNs by HepG2 cells was investigated through confocal analyses. Cells were seeded at a density of 12×10^3 cm^2 on Ibidi µ-Dish (35 mm, Ibidi) and incubated at 37 °C and 5% CO_2 in order to reach confluence. Sor-Mag-SLNs were red-fluorescently stained with DiI (Life Technologies), a lipophilic fluorescent stain for labeling cell membranes and other hydrophobic structures, and thereafter added to the cell culture medium at a concentration of 100 µg mL^{-1}. After 24 h of incubation, the cells were rinsed with PBS and treated for 45 min with LysoTracker (Invitrogen), a fluorescent acidotropic probe for labeling and tracking of acidic organelles (lysosomes) in live cells. Finally, cells were rinsed with PBS, incubated for 10 min with Hoechst 33342 (5 µg mL^{-1}, H1399 Invitrogen) for nucleus counterstaining, and observed with a confocal microscope (C2s, Nikon).

Dynamic Cell Culture and Magnetic Targeting Experiment: Sor-Mag-SLN magnetic targeting experiments in dynamic cell culture conditions were performed using a two syringes perfusion set-up connected to a fluidic unit with programmable switching valves and plastic channel µ-Slides (µ-Slide VI$^{0.4}$, Ibidi) for cell culturing. The home-made air pump system, built with a peristaltic pump linked to a feedback system, allows the pressure input to the syringes and the electrovalves periodic switching to be controlled via software interface. Valve action and silicone tubing ensure continuous and directional cell medium flow inside the microfluidic plastic slide avoiding medium depletion. The whole perfusion set-up was placed in an incubator to ensure physiological temperature condition for the entire duration of the experiment. All the experiments where performed for 4 h at the constant flow rate of 2.3 mL min^{-1} inside the microfluidic channel, with a wall shear stress of about 4 dyn cm^{-2} set after the calibration of the perfusion set-up. These values were chosen considering wall shear stress in small diameter blood vessels (2–3 mm inner diameter) ranging between 1–10 dyn cm^{-2}, as reported in the literature.[55–57] No occlusions of silicon tubing and microfluidic channel due to particle aggregation was observed during the experiments, confirming the excellent stability of the SLNs in the cell culture medium. A scheme of the fluidic set-up is given in Figure 7a. HepG2 cells were seeded at the bottom of two of the six rectangular-shaped microfluidic channels of the µ-Slide, with size 0.4 × 17 × 3.8 mm. All the seeded channels were previously incubated with gelatin (4% in PBS) for 20 min at 37 °C and then washed three times with PBS to improve cell adhesion. Cells (7×10^4 per each channel) were incubated for three days at 37 °C and 5% CO_2 in order to reach confluence before performing experiments. In order to assess targeting efficiency, the syringes were loaded with medium containing red-fluorescently labeled Sor-Mag-SLNs (50 µg mL^{-1}). A permanent neodymium magnet (B_r = 1.32 T) was positioned at the bottom of one of the seeded channels to magnetically target Sor-Mag-SLNs near the area of action of the magnetic field, while the other channel was used as negative control. After 4 h, the experiment was stopped and cells were rinsed with PBS, fixed with paraformaldehyde (4% in PBS), treated with Triton 0.1% X-100 to allow membrane permeabilization, and blocked for 1 h with a goat serum solution (10% in PBS). Thereafter, cultures were incubated with a staining solution containing phalloidin (1:100, Millipore) and DAPI (1:1000, Millipore) to label cytoskeletal f-actin and nuclei, respectively. After extensive PBS rinsing, images were acquired by confocal microscope. An analogous procedure was followed in order to demonstrate selective magnetic-targeted cytotoxic effects of Sor-Mag-SLNs in dynamic conditions. Also in this case, medium containing 50 µg mL^{-1} of Sor-Mag-SLNs was circulated in the system for 4 h. Thereafter, cells were incubated in static conditions for 72 h before performing Live/Dead viability/cytotoxicity assay. Quantitative evaluation of cell mortality was performed by counting EthD-1 positive cells over the total number of cells.

Statistical Analysis: Data were analyzed with one-way ANOVA followed by Bonferroni's post hoc test or two-tailed unpaired *t*-test through KaleidaGraph (Sinergy Software). In all experiments, performed in triplicate, data with p value < 0.05 were considered statistically significant.

Supporting Information

Supporting Information is available from the Wiley Online Library or from the author.

Acknowledgements

Authors gratefully thank Bayer International and Gattefossé Italy, for providing sorafenib and cetyl palmitate, respectively. Moreover, Professor M. D'Orazio (Earth Sciences Department, University of Pisa) is kindly acknowledged for performing ICP-MS analyses. C.I. would like to thank Italian MIUR for financial support through FIRB "RINAME *Rete Integrata per la NAnoMEdicina*" (RBAP114AMK).

Received: April 2, 2015
Revised: May 13, 2015
Published online: June 3, 2015

[1] Y. Hoshida, B. C. Fuchs, K. K. Tanabe, *Curr. Cancer Drug Targets* **2012**, *12*, 1129.
[2] H. B. El-Serag, K. L. Rudolph, *Gastroenterology* **2012**, *132*, 2557.
[3] G. Fattovich, T. Stroffolini, I. Zagni, F. Donato, *Gastroenterology* **2004**, *127*, 35.
[4] D. Schuppan, N. H Afdhal, *Lancet* **2008**, *371*, 838.
[5] J. Bruix, M. Sherman, *Hepathology* **2005**, *42*, 5.
[6] J. M. Llovet, A. M. Di Bisceglie, J. Bruix, B. S. Kramer, R. Lencioni, A. X. Zhu, M. Sherman, M. Schwartz, M. Lotze, J. Talwalkar, G. J. Gores, *J. Natl. Cancer Inst.* **2008**, *100*, 698.
[7] S. Lin, K. Hoffmann, P. Schemmer, *Liver Cancer* **2012**, *1*, 144.
[8] R. Sacco, *Future Oncol.* **2014**, *10*, 2073.
[9] G. M. Keating, A. Santoro, *Drugs* **2009**, *69*, 223.
[10] S. M. Wilhelm, L. Adnane, P. Newell, A. Villanueva, J. M. Llovet, M. Lynch, *Mol. Cancer Ther.* **2008**, *7*, 3129.
[11] S. M. Wilhelm, C. Carter, L. Tang, D. Wilkie, A. McNabola, H. Rong, C. Chen, X. Zhang, P. Vincent, M. McHugh, Y. Cao, J. Shujath, S. Gawlak, D. Eveleigh, B. Rowley, L. Liu, L. Adnane, M. Lynch, D. Auclair, I. Taylor, R. Gedrich, A. Voznesensky, B. Riedl, L. E. Post, G. Bollag, P. A. Trail, *Cancer Res.* **2004**, *64*, 7099.
[12] L. S. del Burgo, J. L. Pedraz, G. Orive, *Drug Discovery Today* **2014**, *19*, 1659.
[13] W. Mehnert, K. Mäder, *Adv. Drug Delivery Rev.* **2001**, *47*, 165.
[14] P. Blasi, S. Giovagnoli, A. Schoubben, C. Puglia, F. Bonina, C. Rossi, M. Ricci, *Int. J. Pharmaceut.* **2011**, *419*, 287.
[15] A. H. Lu, E. L. Salabas, F. Schüth, *Angew. Chem. Int. Ed* **2007**, *46*, 1222.
[16] M. Mahmoudi, S. Sant, B. Wang, S. Laurent, T. Sen, *Adv. Drug Delivery Rev.* **2011**, *63*, 24.
[17] L. H. Reddy, J. L. Arias, J. Nicolas, P. Couvreur, *Chem. Rev.* **2012**, *112*, 5818.
[18] S. Laurent, D. Forge, M. Port, A. Roch, C. Robic, L. Vander Elst, R. N. Muller, *Chem. Rev.* **2008**, *108*, 2064.
[19] Y. Gossuin, P. Gillis, A. Hocq, Q. L. Vuong, A. Roch, *WIREs Nanomed. Nanobiotechnol.* **2009**, *1*, 299.
[20] R. Qiao, C. Yang, M. Gao, *J. Mater. Chem.* **2009**, *19*, 6274.
[21] A. J. L. Villaraza, A. Bumb, M. W. Brechbiel, *Chem. Rev.* **2010**, *110*, 2921.
[22] H. Kim, H. M. Dae, C. Park, E. O. Kim, D. Kim, I. H. Kim, Y. H. Kim, Y. Choi, *J. Mater. Chem.* **2011**, *21*, 7742.
[23] A. Taylor, A. Herrmann, D. Moss, V. Sée, K. Davies, S. R. Williams, P. Murray, *PLoS ONE* **2014**, *9*, e100259.
[24] M. Rohrer, H. Bauer, J. Mintorovitch, M. Requardt, H. J. Weinmann, *Invest. Radiol.* **2005**, *49*, 715.
[25] C. W. Jung, P. Jacobs, *Magn. Reson. Imaging* **1995**, *13*, 661.
[26] J. Qin, S. Laurent, Y. S. Jo, A. Roch, M. Mikhaylova, Z. M. Bhujwalla, R. N. Muller, M. Muhammed, *Adv. Mater.* **2007**, *19*, 1874.
[27] M. Cervello, D. Bachvarov, N. Lampiasi, C. Cusimano, A. Azzolina, J. A. McCubrey, G. Montalto, *Cell Cycle* **2012**, *11*, 2843.
[28] F. M. Gu, Q. L. Li, Q. Gao, J. H. Jiang, X. Y. Huang, J. F. Pan, J. Fan, J. Zhou, *World J. Gastroenterol.* **2011**, *17*, 3922.
[29] N. Schleich, F. Danhier, V. Préat, *J. Controlled Release* **2015**, *198*, 35.
[30] C. Niu, Z. Wang, G. Lu, T. M. Krupka, Y. Sun, Y. You, W. Song, H. Ran, P. Li, Y. Zheng, *Biomaterials* **2013**, *34*, 2307.
[31] N. Schleich, P. Sibret, P. Danhier, B. Ucakar, S. Laurent, R. N. Muller, C. Jérôme, B. Gallez, V. Préat, F. Danhier, *Int. J. Pharm.* **2013**, *447*, 94.
[32] V. P. Torchilin, *Adv. Drug Delivery Rev.* **2012**, *64*, 302.
[33] T. M. Allen, P. R. Cullis, *Adv. Drug Delivery Rev.* **2013**, *65*, 36.
[34] K. Cho, X. Wang, S. Nie, Z. G. Chen, D. M. Shin, *Clin. Cancer Res.* **2008**, *14*, 1310.
[35] D. H. Kim, M. D. Kim, C. W. Choi, C. W. Chung, S. H. Ha, C. H. Kim, Y. H. Shim, Y. I. Jeong, D. H. Kang, *Nanoscale Res. Lett.* **2012**, *7*, 91.
[36] C. F. Wang, E. M. Mäkilä, M. H. Kaasalainen, D. Liu, M. P. Sarparanta, A. J. Airaksinen, J. J. Salonen, J. T. Hirvonen, H. A. Santos, *Biomaterials* **2014**, *35*, 1257.
[37] H. Zhang, F. M. Zhang, S. J. Yan, *Int. J. Nanomed.* **2012**, *7*, 2901.
[38] Z. Zhang, B. Niu, J. Chen, X. He, X. Bao, J. Zhu, H. Yu, Y. Li, *Biomaterials* **2014**, *35*, 4565.
[39] A. J. Mieszawska, J. T. Kim, A. Gianella, I. van Rooy, B. Priem, M. P. Labarre, C. Ozcan, D. P. Cormode, A. Petrov, R. Langer, O. C. Farokhzad, Z. A. Fayad, W. J. M. Mulder, *Bioconjugate Chem.* **2013**, *24*, 1429.
[40] J. Chen, A. Y. Sheu, W. Li, Z. Zhang, D. H. Kim, R. J. Lewandowski, R. A. Omary, L. D. Shea, A. C. Larson, *J. Controlled Release* **2014**, *184*, 10.
[41] J. Liu, B. Boonkaew, J. Arora, S. H. Mandava, M. M. Maddox, S. Chava, C. Callaghan, J. He, S. Dash, V. T. John, B. R. Lee, *J. Pharm. Sci.* **2015**, *104*, 1187.
[42] L. Zhang, F. Gong, F. Zhang, J. Ma, P. Zhang, J. Shen, *Int. J. Nanomed.* **2013**, *8*, 1517.
[43] J. Panyam, M. M. Dali, S. K. Sahoo, W. Ma, S. S. Chakravarthi, G. L. Amidon, R. J. Levy, V. Labhasetwar, *J. Controlled Release* **2003**, *91*, 173.
[44] W. Mehnert, K. Mäden, *Adv. Drug Delivery Rev.* **2001**, *47*, 165.
[45] R. H. Müller, M. Radtke, S. A. Wissing, *Int. J. Pharmaceut.* **2002**, *242*, 121.
[46] R. H. Müller, K. Mäder, S. Gohla, *Eur. J. Pharm. Biopharm.* **2000**, *50*, 161.
[47] J. H. Ryu, S. Lee, S. Son, S. H. Kim, J. F. Leary, K. Choi, I. C. Kwon, *J. Controlled Release* **2014**, *190*, 477.
[48] H. He, A. David, B. Chertok, A. Cole, K. Lee, Z. Zhang, J. Wang, Y. Huang, V. C. Yang, *Pharm. Res.* **2013**, *30*, 2445.
[49] J. Xie, S. Lee, X. Chen, *Adv. Drug Delivery Rev.* **2010**, *62*, 1064.
[50] J. E. Rosen, L. Chan, D. B. Shieh, F. X. Gu, *Nanomedicine: NBM* **2012**, *8*, 275.
[51] W. J. Heinz, K. Kahle, A. Helle-Beyersdorf, D. Schirmer, U. Lenker, D. Keller, P. Langmann, H. Klinker, *Cancer Chemioth. Pharm.* **2010**, *68*, 239.
[52] R. Kimmich, E. Anoardo, *Progr. Nucl. Magn. Reson. Spectrosc.* **2004**, *44*, 257.
[53] H. Y. Carr, E. M. Purcell, *Phys. Rev.* **1954**, *94*, 630.
[54] S. Meiboom, D. Gill, *Rev. Sci. Instrum.* **1958**, *29*, 688.
[55] C. Williams, T. M. Wick, *Tissue Eng.* **2004**, *10*, 5.
[56] J. Ando, K. Yamamoto, *Circ. J.* **2009**, *73*, 1983.
[57] H. Yang, X. Xiong, L. Zhang, C. Wu, Y. Liu, *Int. J. Nanomed.* **2011**, *6*, 2043.